[6]Wood, D. H., "A Three-Dimensional Analysis of Stall-Delay on Horizontal-Axis Wind Turbine," *Journal of Wind Engineering and Industrial Aerodynamics*, Vol. 37, 1991, pp. 1–14.

[7]Cebecci, T., *An Engineering Approach to the Calculation of Aerodynamic Flows*, Springer, Berlin, 1999, pp. 51–62.

[8]Banks, W. H. H., and Gaad, G. E., "Delaying Effect of Rotation on Laminar Separation," *AIAA Journal*, Vol. 1, No. 4, 1963, pp. 941, 942.

S. K. Aggarwal
Associate Editor

Microstructured Hydrophobic Skin for Hydrodynamic Drag Reduction

Ashwin K. Balasubramanian,* Adam C. Miller,*
and Othon K. Rediniotis†
Texas A&M University, College Station, Texas 77843

Introduction

An important issue in the development of underwater vehicles and surface ships is devising novel ways to reduce hydrodynamic drag. Drag reduction for small underwater vehicles can alleviate the need for expensive power sources to achieve their specified range and endurance. Large surface and underwater vessels can use drag reduction to extend their ranges, or reduce the amount of fuel consumed or carried. One approach to skin-friction drag reduction involves using a film or discrete layer of air at the wall to take advantage of the greatly lower viscosity of a near-wall gas phase.

Recent attempts to control the production of turbulence near a wall have been reviewed by Bushnell,[1] Bandopadhyay,[2,3] and Gad-el-Hak.[4] The experiments of Bruse et al.[5] show that it is possible to achieve a net drag reduction of 10% with new hybrid surfaces. Jung et al.[6] have numerically shown that a span wise oscillation can lead to 40% reduction on near-wall vorticity fluctuations and drag. Bandopadhyay[7] has used "selective suction and injection" for the control of turbulence in a boundary layer. Wall pressure measurements indicated a slight reduction, which tended to wash out when averaged over more than 500 individual realizations of spectra. Other researchers have studied the slip mechanism in polymer melts and solutions, which cause flow instabilities due to surface interactions.[8]

Here we present findings from our work on a new technology for hydrodynamic drag reduction. It involves a microstructure skin that emulates the surface structure of lotus leaves.[9] A scanning electron microscope picture of the surface is shown in Fig. 1, illustrating the distribution of microstructures on it. It has been observed that beneficial results are obtained if the following conditions are generally met: 1) The nature and character of the surface are selected so that the wetting angle, between a water droplet and the surface, is at a maximum and 2) the contact of the water droplet with the surface has to occur over a minimum area.[10,11] For the surface we tested, when water is deposited on this surface, the combination of the microstructures and the water surface tension traps air between the microstructures. Thus, when water is flowing on the surface, effectively it rides on a layer of air. Because the dynamic viscosity of air (0.000018 kg/m · s) is significantly smaller than that of water (0.001 kg/m · s), the skin friction of the surface and, thus, the hydrodynamic drag are reduced. The objective of this work is to test this artificial surface for quantifying its skin-friction reduction properties. A set of experiments was performed to explore the former and the details are discussed.

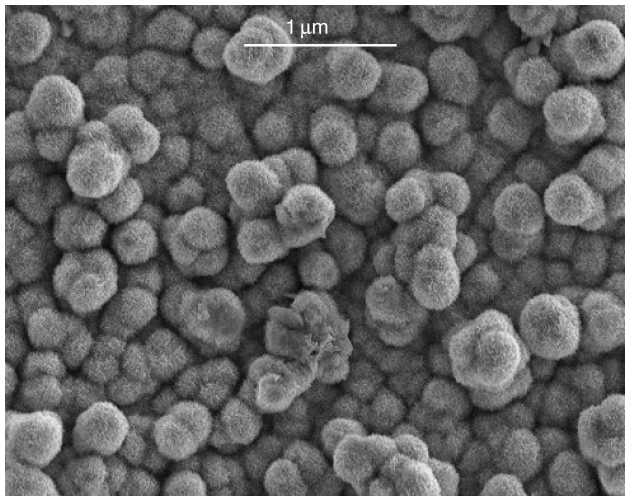

Fig. 1 SEM pictures of microstructure skin surface.

Experimental Setup, Procedures, Uncertainty Analysis, and Discussion of Results

Experiment 1: Flat Plate Model

Particle image velocimetry (PIV) was performed to quantify the effects of the coating/skin on the boundary-layer velocity profile over a flat plate. A flat plate, measuring 55 cm long × 15 cm wide, was tested with and without the coating. The leading edge of the plate was properly shaped to prevent flow separation. In the experiment performed, the flat plate was mounted inside a water tunnel, and the flowfield was seeded with silicon carbide particles, 1.5 μm in diameter. The water-tunnel test section measures 60 cm in length and 15.5 × 19.5 cm in cross section. The water tunnel is capable of operating at speeds up to 470 mm/s. For the current experiment performed, the tunnel was operated at a freestream velocity of 100 mm/s. A laser sheet of power 25 W was used to illuminate the flow. The images were captured using a high-speed Phantom charge-coupled device camera capable of operating at a maximum frame rate of up to 3000 frames per second. The camera was operated at a frame rate of 576 frames per second, and a total of 576 consecutive images were captured. The camera was focused on a 5 × 5 mm area in the boundary layer of the flat plate (view area oriented perpendicular to the plate and parallel to the freestream direction), at a horizontal distance of 44 cm from the leading edge of the plate. Each 512 × 512 pixel image was analyzed to obtain the velocity distribution.

The microstructure skin used in these experiments was generated from two different products, the details of which are as follows: The first product is a Bolta copper foil, which, before processing, behaves like any normal copper foil. The second product is Dynasilan liquid, with which we treated the foil. This liquid is a solution of flourosilane in ethanol. The processing of the foil with the liquid is as follows: A diluted solution (20% vol Dynasilan, 80% vol ethanol) is sprayed on the foil's surface to wet it completely, and the foil is subsequently cured in an oven for one hour at 100°C. After heat treatment, the microstructures on the surface of the foil comprise two different layers, with the microstructures themselves having a height and width of about 300 nm. The surface of the skin was analyzed using an scanning electron microscope (SEM), and Fig. 1 shows the surface of the microstructure skin as viewed through an SEM.

Uncertainty Analysis for Experiment 1

An uncertainty analysis was performed for the PIV measurements using the method described by Kline and McClintock.[12] The

Received 18 June 2002; revision received 1 February 2003; accepted for publication 1 July 2003.

*Graduate Research Assistant, Department of Aerospace Engineering.

†Associate Professor, Department of Aerospace Engineering. Associate Fellow AIAA.

velocity vectors were calculated from the particle images using cross-correlation algorithms with subpixel accuracy.[13,14] The following relation defines the velocity:

$$V = \mathrm{PPF} \cdot \mathrm{FR} \cdot \mathrm{MMP} \tag{1}$$

where pixel per frame (PPF) is the magnitude of the displacement (in pixels), frame rate (FR) is the camera frame rate (1/s), and millimeter per pixel (MMP) is the conversion factor. To perform the uncertainty analysis, the following assumptions were made:

1) Each one of the mentioned variables is independent of each other.

2) Each one of the variables has a Gaussian distribution.

3) The seeding particles are assumed to follow the flow. The particles used were 1.5 μm in diameter and neutrally buoyant, and there was no unsteadiness in the flow. Therefore, we feel that this assumption is valid.

The uncertainty of the data may be expressed as

$$wt = \sqrt{\left(\frac{\partial V}{\partial \mathrm{PPF}} \cdot w_{\mathrm{ppf}}\right)^2 + \left(\frac{\partial V}{\partial \mathrm{FR}} \cdot w_{\mathrm{fr}}\right)^2 + \left(\frac{\partial V}{\partial \mathrm{MMP}} \cdot w_{\mathrm{mmp}}\right)^2} \tag{2}$$

where w_{ppf} is the uncertainty in the estimation of the displacement (in pixels), w_{fr} is the uncertainty in the frame rate of the camera (or equivalently in the time between frames), and w_{mmp} is the uncertainty in the estimation of the MMP factor. For the experiments presented here, the values of the parameters were estimated to be PPF = 10, FR = 576, MMP = 0.0117, $w_{\mathrm{ppf}} = 0.1$, $w_{\mathrm{fr}} = 0.5$, and $w_{\mathrm{mmp}} = 0.00017$. When these values are substituted into Eq. (2), the uncertainty in the velocity measurement was found to be 1.1765% of the freestream velocity.

Results and Discussion for Experiment 1

The velocity fields were generated for both the coated and uncoated plates. Figure 2 shows the velocity vector plots for both cases. It can be seen from these vector plots that, in the case of the plate with the coating, even the particles on the surface of the plate (or at least as close to it as our hardware could distinguish) are moving with a finite velocity. Also, the coating on the plate seems to reduce the boundary layer-thickness significantly.

From these vector plots, the average (within the length of the image) boundary-layer profiles for both cases were generated and nondimensionalized. Figure 3 shows the average nondimensional velocity profiles for the coated and uncoated plates as a function of distance from the surface of the plate, along with the corresponding Blasius boundary-layer profile. From the Blasius theory, the skin friction and drag relate directly to the momentum thickness. The momentum thicknesses were calculated from these graphs as

$$\delta_2 = \int \frac{U}{U_{\max}}\left(1 - \frac{U}{U_{\max}}\right) \mathrm{d}y$$

with the integration performed from $y = 0$ to 3.9375 mm. Simpson's numerical method of integration was used to integrate the nondimensional velocity profiles to obtain the momentum thickness for the coated and uncoated plates, respectively:

$$\delta_{2(\mathrm{coated})} = 0.404048 \text{ mm}, \qquad \delta_{2(\mathrm{uncoated})} = 0.507588 \text{ mm}$$

The ratio $K = \delta_{2(\mathrm{coated})}/\delta_{2(\mathrm{uncoated})} = 0.796$ is proportional to the drag ratio for the two plates. It can be seen that a drag reduction of around 20% has been achieved by coating the plate with the artificial surface.

Experiment 2: Ellipsoid Model

A second water-tunnel experiment was performed to quantify the integral drag reduction benefits gained through the use of the skin. Toward that goal, a 6-to-1 ellipsoidal model, 3 ft (0.9144 m) long, was fabricated in our rapid prototyping machine out of acrylonitrile butadiene styrene (ABS) plastic. The model was constructed in six pieces, as shown in Fig. 4, which were then assembled to form the final model with each piece fitting onto its adjacent pieces perfectly, without any gaps or steps. The final assembled model has high geometric precision (order of 0.005 in.) and is structurally strong.

The drag measurements were obtained using a balance created explicitly for this experiment. Figure 5 shows a schematic of the experimental setup. A linear rectangular air bearing was used to ensure that accuracy is not lost due to the friction. From Fig. 5 it can be seen that the stationary portion of the air bearing was

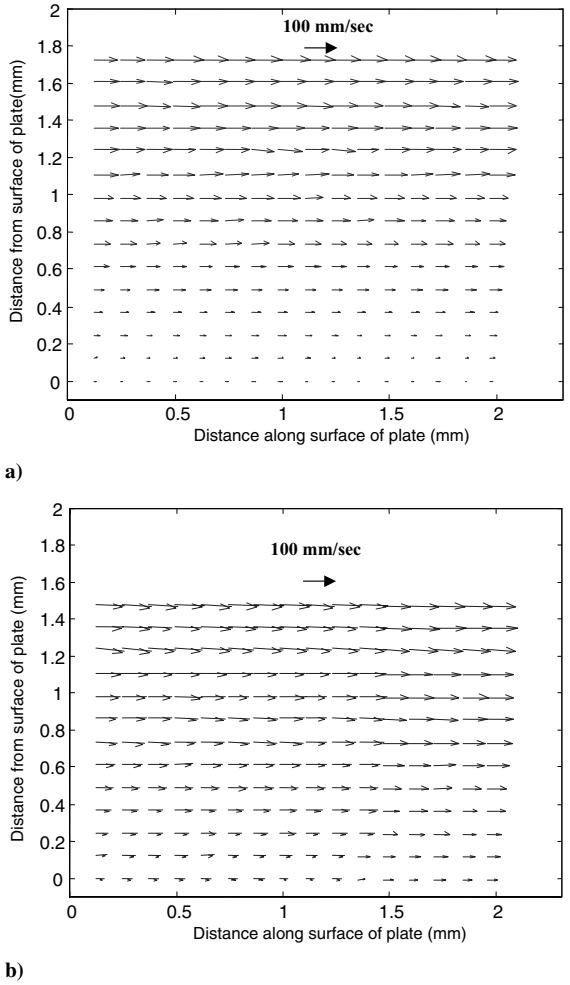

Fig. 2 Velocity vector plot for the plate a) without coating and b) with coating.

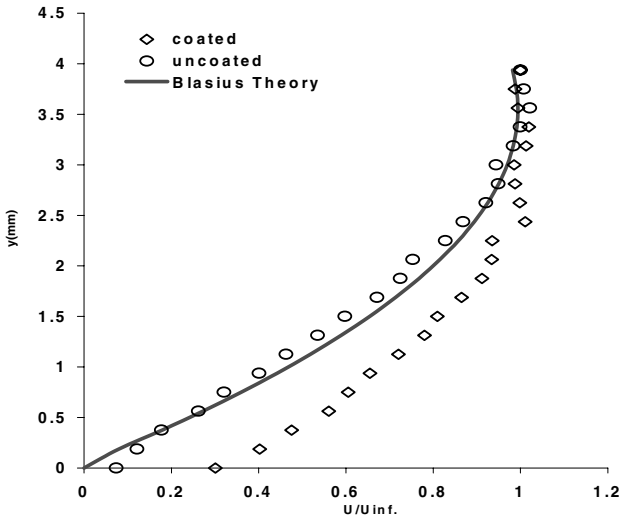

Fig. 3 Nondimensional velocity profiles in the boundary layer of the coated and uncoated flat plate.

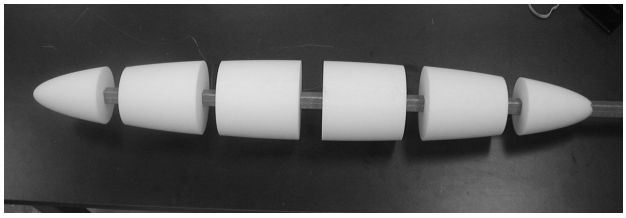

Fig. 4 Six components of the model on the fiberglass square backbone.

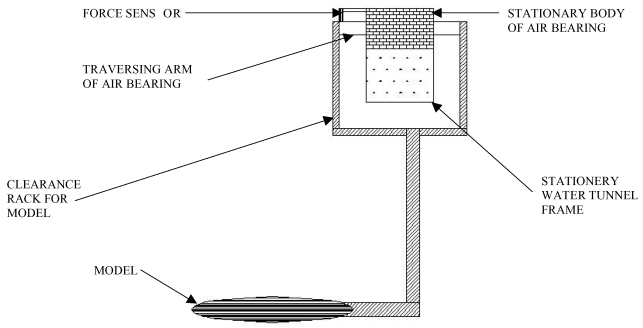

Fig. 5 Setup for the test of the fiberglass model.

attached to the water tunnel. The clearance rack is supported from the traversing portion of the air bearing. This rack holds the sting that attaches to the rear of the ellipsoid model. The sting is designed to allow the model to be tested at various angles of attack in the water tunnel. A beam force sensor located on the traversing arm of the air bearing measured the total drag force. This force beam sensor can be interchanged to achieve the highest possible accuracy at a given angle of attack. To maintain accuracy at lower angles of attack a smaller range force beam sensor is used. For higher angles of attack and, thus, greater drag forces, a larger range sensor was used to ensure that the sensor is not overloaded and damaged. The experiments were conducted in the Aerospace Engineering 2×3 ft water tunnel. This is a free-surface water tunnel with test-section dimensions of 2×3 ft in cross section and 7 ft in length, a contraction ratio of 6:1, and a maximum attainable speed of 4 ft/s (1.2 m/s).

Two sets of drag measurement tests were conducted with the model. The first set was performed on the uncoated model, at three different freestream velocities, 0.2, 0.4, and 0.6 m/s, and two angles of attack, 0 and 8 deg. The second set of tests was performed on the skin-coated model under the same conditions of freestream velocities and angles of attack as the uncoated case. The skin coating covered the entire surface area of the ellipsoidal model. Higher angles of attack could not be tested due to the limitations of the water-tunnel test section and the size of the model. The critical Reynolds number for flow over a 6-to-1 prolate spheroid has been established as 2.5×10^6 based on previous work.[15] Based on this assumption, the Reynolds numbers under which our experiments were conducted suggest that the flow is laminar. Also, at 0- and 8-deg angle of attack, the critical Reynolds number value is fully valid, and hence, trip strips were not used to counter any Reynolds-number-sensitive separations.

Uncertainty Analysis for Experiment 2

An uncertainty analysis was performed for the drag measurements using the method described by Kline and McClintock.[12] The nondimensional drag coefficient is calculated from the measured drag, which is measured as a voltage output from the force transducers. The following relation defines the nondimensional drag coefficient:

$$C_D = D \Big/ \tfrac{1}{2} \cdot \rho \cdot V^2 \cdot S \tag{3}$$

where D is the drag measured from the transducer voltage via calibration, ρ is the density of water, V is the freestream velocity, and S is the reference area used, which in our case is the model minor cross-sectional area (circle with a diameter of 0.5 ft). To perform the uncertainty analysis, the following assumptions were made:

1) Each one of the mentioned variables is independent of each other.

2) Each one of the variables has a Gaussian distribution.

3) Unsteadiness in the flow is neglected, and the uncertainty in the drag is assumed to be the same as the uncertainty in the transducer specification sheet, which is a root mean square of the individual uncertainties due to nonlinearity, nonrepeatability, and hysterisis.

The uncertainty of the data may be expressed as

$$wt = \sqrt{\left(\frac{\partial C_D}{\partial D} \cdot w_D\right)^2 + \left(\frac{\partial C_D}{\partial \rho} \cdot w_\rho\right)^2 + \left(\frac{\partial C_D}{\partial V} \cdot w_V\right)^2 + \left(\frac{\partial C_D}{\partial S} \cdot w_S\right)^2} \tag{4}$$

where w_D is the uncertainty in the measurement of the drag (in newtons), w_ρ is the uncertainty in the density of the water (in kilograms per cubic meter), w_V is the uncertainty in the freestream velocity (in meters per second), and w_S is the uncertainty in the estimation of the reference area used for the calculations (in square meters). For the experiments presented here, a typical set of values for the parameters are $D = 1.8$ N, $\rho = 1000$ kg/m^3, $V = 0.6$ m/s, $S = 0.1095$ m^2, $w_D = 0.0023$ N, $w_\rho = 0.03$ kg/m^3, $w_V = 0.0012$ m/s, and $w_S = 1.613 \times 10^{-8}$ m^2. When these values are substituted into Eq. (4), the uncertainty in the nondimensional drag coefficient measurement was found to be 0.42% of the calculated C_D.

Results and Discussion for Experiment 2

Figure 6 shows the drag coefficient comparison between the coated and uncoated model at 0- and 8-deg angle of attack at different Reynolds numbers. From the total drag values recorded by the force sensor, the percentage drag reduction by coating the model with the skin is calculated for both angles of attack. Figure 7 shows the percentage drag reduction as a function of the Reynolds number for both angles of attacks. From Fig. 7, it can be seen that around 14% drag reduction is achieved by coating the model surface with the skin, at 0-deg angle of attack, and around 10% drag reduction is achieved with the skin, at 8-deg angle of attack. The lower drag reduction at 8-deg angle of attack results because less of the drag is a result of the skin friction and more from pressure drag.

Loss of Hydrophobicity

As stated earlier, the skin partially loses its hydrophobicity, as it remains submerged in water for a long time. This is shown in Fig. 8, which shows the drag reduction percentage as a function of time for a freestream velocity of 0.6 m/s, at 0-deg angle of attack. As shown in Fig. 8, after long periods of time submerged in water, the benefits of the skin are reduced. However, the percentage drag reduction seems to reach a steady state at a level of about 10%. The effectiveness of the skin is regained if the skin is removed from the water for a short

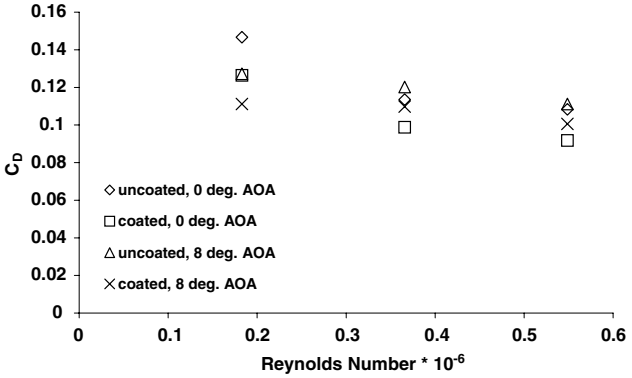

Fig. 6 Drag coefficient comparison between coated and uncoated model at 0- and 8-deg angle of attack.

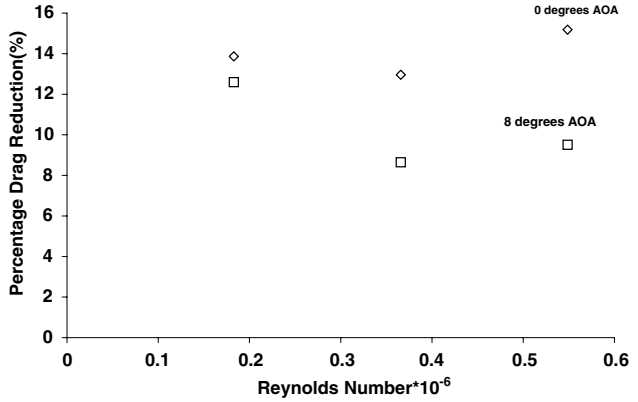

Fig. 7 Percentage drag reduction on the ellipsoid with coating.

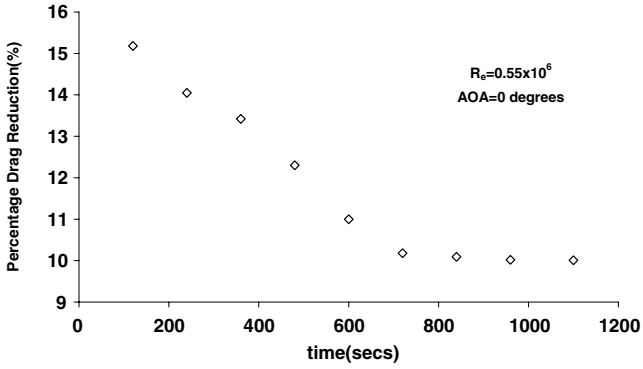

Fig. 8 Percentage drag reduction as a function of time.

period of time and is allowed to dry. The results presented here are for models that have remained submerged for 1100 s.

Conclusions

A hydrophobic coating/skin was tested to quantify its effectiveness as a hydrodynamic drag reduction device. PIV performed on a flat plate, with and without the coating, showed a 20% drag reduction induced by the coating. Drag measurement tests, conducted on a 3-ft-long ellipsoid model in the water tunnel, showed 14 and 10% drag reductions at 0- and 8-deg model angle of attack, respectively. Drag reduction levels drop with time, apparently approaching a limiting value after 15 min.

Acknowledgments

The authors thank C. Neinhuis of the University of Bonn and his students for helping with initial samples of the skin and providing information about suppliers of the raw materials for the fabrication of the skin.

References

[1]Bushnell, D. M., "Turbulent Drag Reduction for External Flows," AIAA Paper 83-0227 and AIAA Paper 83-0231, Jan. 1983.

[2]Bandopadhyay, P. R., "REVIEW—Mean Flow in Turbulent Boundary Layers Distributed to Alter Skin Friction," *Journal Fluids Engineering*, Vol. 108, 1986, pp. 127–140.

[3]Bandopadhyay, P. R., "Convex Curvature Concept of Viscous Drag Reduction," *Viscous Drag Reduction in Boundary Layers*, edited by D. M. Bushnell and J. N. Hefner, Vol. 123, Progress in Aeronautics and Astronautics, AIAA, Washington, DC, 1990, pp. 285–324.

[4]Gad-el-Hak, M., "Flow Control," *Applied Mechanics Reviews*, Vol. 9, 1989, pp. 447–468.

[5]Bruse, M., Bechert, D. W., Van der Hoeven, J. G. T., Hage, W., and Hoppe, G., "Experiments with Conventional and Novel Adjustable Drag-Reducing Surfaces," *Near-Wall Turbulent Flows*, edited by R .M. C. So, C. G. Speziale, and B. E. Launder, Elsevier, New York, 1993, pp. 719–738.

[6]Jung, W. J., Mangiavacchi, N., and Akhavan, R., "Suppression of Turbulence in Wall-Bounded Flows by High-Frequency Spanwise Oscillations," *Physics of Fluids*, Vol. 4, No. 8, 1992, pp. 1605–1607.

[7]Bandopadhyay, P. R., "Development of a Microfabricated Surface for Turbulence Diagnostics and Control," *Application of Microfabrication to Fluid Mechanics*, FED Vol. 1997, American Society of Mechanical Engineers, Fairfield, NJ, 1994, pp. 63–70.

[8]William, B. B., "Wall Slip and Boundary Effects in Polymer Shear Flows," Ph.D. Dissertation, Dept. of Chemical Engineering, Univ. of Wisconsin, Madison, WI, May 2000.

[9]Barthlott, W., and Neinhuis, C., "Purity of the Sacred Lotus, or Escape from Contamination in Biological Surfaces," *Planta*, Vol. 202, 1997, pp. 1–8.

[10]Neinhuis, C., and Barthlott, W., "Characterization and Distribution of Water-Repellent, Self-Cleaning Plant Surfaces," *Annals of Botany*, Vol. 79, 1997, pp. 667–677.

[11]Adam, N. K., "Principles of Water-Repellency," *Waterproofing and Water-Repellency*, edited by J. L. Moilliet, Elsevier, Amsterdam, 1963, pp. 1–147.

[12]Kline, S. J., and McClintock, F. A., "Describing Uncertainties in Single-Sample Experiments," *Mechanical Engineering*, Vol. 75, Jan. 1953, pp. 3–88.

[13]Willert, C. E., and Gharib, M., "Digital Particle Image Velocimetry," *Experiments in Fluids*, Vol. 10, 1991, pp. 181–193.

[14]Singh, K., "Development of Image Processing Algorithms for an Improved Particle Image Velocimetry System," M.S. Thesis, Dept. of Aerospace Engineering, Texas A&M Univ., College Station, TX, May 1998.

[15]Ahn, S., "An Experimental Study of Flow over a 6 to 1 Prolate Spheroid at Incidence," Ph.D. Dissertation, Aerospace Engineering Dept., Virginia Polytechnic Inst. and State Univ., Blacksburg, VA, Oct. 1992.

P. R. Bandyopadhyay
Associate Editor

Optimized Boundary Treatment of Curved Walls for High-Order Computational Aeroacoustics Schemes

Jonghoon Bin,* Cheolung Cheong,† and Soogab Lee‡
Seoul National University,
Seoul 151-742, Republic of Korea

Introduction

AN accurate simulation of acoustic scattering and radiation from arbitrary bodies is one of the important goals in the field of computational aeroacoustics. These problems require not only a high-resolution numerical scheme but also accurate boundary treatment. In this Note, we develop a high-order wall boundary treatment that can be readily applied with a high-order finite difference in computational aeroacoustics.

There are mainly three types of approaches for treating complex geometries. The first is to use a conventional structured grid, the second is to make use of unstructured grids that create irregular numerical interfaces all over the physical domain, and the last type is to use so-called Cartesian grid methods.[1–11] Most of these schemes have been developed for steady-state, transonic flow or low-order accuracy. However, acoustic waves are intrinsically unsteady, and

Received 20 May 2001; revision received 6 March 2003; accepted for publication 10 September 2003.

*Ph.D. Candidate, School of Mechanical and Aerospace Engineering; mrbin@snu.ac.kr.

†BK21 Postdoctoral Research Associate, School of Mechanical and Aerospace Engineering; accu99@snu.ac.kr.

‡Professor, School of Mechanical and Aerospace Engineering; solee@plaza.snu.ac.kr. Senior Member AIAA.